

Fatigue and fretting fatigue life prediction of double-lap bolted joints using continuum damage mechanics-based approach

Ying Sun¹, George Z Voyiadjis², Weiping Hu^{1,2}, Fei Shen¹
and Qingchun Meng¹

Abstract

Fatigue and fretting fatigue are the main failure mode in bolted joints when subjected to cyclic load. Based on continuum damage mechanics, an elastic–plastic fatigue damage model and a fretting fatigue damage model are combined to evaluate the fatigue property of bolted joints to cover the two different failure modes arisen at two possible critical sites. The predicted fatigue lives agree well with the experimental results available in the literature. The beneficial effects of clamping force on fatigue life improvement of the bolted joint are revealed: part of the load is transmitted by friction force in the contact interface, and the stress amplitude at the critical position is decreased due to the reduction in the force transmitted by the bolt. The negative effect of fretting damage on the bolted joint is also captured in the simulation.

Keywords

Fatigue damage, fretting fatigue, double-lap bolted joints, continuum damage mechanics, finite element

Introduction

Bolted joints are widely used in aircraft structures to transmit loads from one structural component to other components. The fastener hole in the bolted joint is prone to be a critical position under cyclic loading due to the high stress concentration at the hole edge. In order to overcome this drawback and improve the fatigue property of joints, application of clamping force is always adopted as an effective method. Experiments (Chakherlou et al., 2011; Esmacili et al., 2014b) show that the fatigue life of metallic double shear joint can be increased as much as 3–7 times

¹School of Aeronautics Science and Engineering, Beihang University, Beijing, China

²Department of Civil and Environmental Engineering, Louisiana State University, Baton Rouge, USA

Corresponding author:

Weiping Hu, School of Aeronautics Science and Engineering, Room D604, New Main Building, 37th Xueyuan Road, Beihang University, Beijing 100191, China.

Email: huweiping@buaa.edu.cn

according to the levels of clamping force. However, the clamped bolted joints may suffer from fretting wear at the surface of plate which easily results in fretting fatigue damage. Fretting fatigue is defined as fatigue phenomenon that occurs on the contacting surfaces of the components due to the small relative displacements between two components. The fretting damage can significantly reduce the fatigue life of the components, and during fretting conditions cracks can initiate at low stresses well below the fatigue limit of nonfretted materials (Endo, 1981; Endo et al., 1969). Therefore, there are two competitive modes in the failure of bolted joints: fatigue failure initiate at the hole edge and fretting fatigue failure initiate at the plate surface.

According to the studies performed by Chakherlou et al. (2011) and Oskouei and Ibrahim (2012), failure mode of the double-lap bolted joints was found to be strongly dependent on the applied tightening torque on the bolt and the alternating load on the plate. The results show that the joints usually experience a fatigue failure with crack initiations from the hole edge due to stress concentration when the cyclic load is heavier; while the joints easily suffer from fretting fatigue with crack initiations on the contacting surface of plate away from the hole when the cyclic load is relatively slight. Meanwhile, the clamping force associated with tightening torque may bring changes between two failure modes. Because of this complicated mechanism of failure, the studies on fatigue and fretting damage of bolted joints mainly rely upon experimental tests.

Since the bolted joints may suffer from different failure mode of fatigue and fretting fatigue, it is difficult to fully describe the failure mode and accurately predict the fatigue life. Esmaeili et al. (2014a) used several multiaxial fatigue criteria to predict fatigue life of bolted joints in order to evaluate the effect of clamping force. However, those fatigue criteria neglected the fretting damage between the contact surfaces and failed to predict the fretting fatigue failure. Compared to the analysis of plain fatigue problem the fretting fatigue is more complex. The primary variables in fretting fatigue are generally considered as contact pressure, slip amplitude, and coefficient of friction (Vingsbo and Söderberg, 1988). A typical fretting configuration of the round on flat (Szolwinski and Farris, 1998) is widely studied to reveal the damage mechanism and the effect of several factors (Araújo and Nowell, 2002; Ding et al., 2014; Madge et al., 2007; Shen et al., 2015b; Zhu et al., 2013), while the fretting in bolted joints is not yet well researched. The development of damage mechanics provides an opportunity to solve this problem. Ferjaoui et al. (2015) used a continuum damage mechanics (CDM)-based approach to the fretting fatigue life of double-lap bolted joint. The approach successfully captured the fretting crack initiation location and lifetime to failure. However, they do not consider the fatigue failure occurring at the hole edge of the bolted joint. This paper aims to analyze those two failure modes simultaneously, to investigate the condition inducing the transition of these two failure modes and to present some characteristics of damage evolution in the failure process of bolted joints.

CDM defines a continuous damage variable D as a measurement of the number of microcracks and microvoids in material to describe the deterioration of materials. Based on the theory of thermodynamics, damage evolution laws combined with damage-coupled elasto-plastic or visco-plastic constitutive models can be derived to model the damage evolution of ductile, fatigue, creep, creep-fatigue, and so on. The details of CDM can be found in the publications by Kachanov (1986), Lemaitre and Chaboche (1990), Lemaitre and Rodrigue (2005), Voyiadjis and Kattan (2005), as well as Murakami (2012). Moreover, the CDM has been extended to describe the damage evolution of anisotropic damage in metal matrix composites (Echle and Voyiadjis, 1999; Voyiadjis and Echle, 1998; Voyiadjis and Thiagarajan, 1995) and to describe the damage evolution of micro-crack distributions in composites (Voyiadjis and Kattan, 2006, 2008). Two kinds of CDM-based approaches are usually applied in practical fatigue damage problems. One is the uncoupled approach, which is used by integrating the damage evolution law without counting the coupling

effect between the damage field and the stress field. The other is the coupled approach, which is applied to accumulate the damage via iteration calculation based on the damage evolution law. The damage-coupled constitutive models often need to be implemented by virtue of finite element method, and the damage is accumulated cycle by cycle to take account of the material degradation and stress redistributions (Lemaitre and Rodrigue, 2005).

In this paper, the damage-coupled Chaboche plasticity constitutive model (Lemaitre and Chaboche, 1990) is used to represent the material behavior, which is implemented by user material subroutine in ABAQUS. The coupled elastic–plastic fatigue damage evolution is analyzed to predict the fatigue failure occurring at the hole edge. At the same time, an uncoupled fretting damage model developed by Ferjaoui et al. (2015) is used to evaluate the fretting fatigue failure initiating at the contact surface of plate. The predicted life and crack initiation position are in good agreement with the experimental results available in literature. The effect of clamping force and coefficient of friction on fatigue damage and fretting fatigue damage of the bolted joint are also discussed and the interaction mechanism is also presented.

Fatigue experiments

The experiments of double-lap bolted joint specimens performed by Oskouei and Ibrahim (2012) are simulated in this paper. A brief overview of the experiment is presented here to clearly illustrate the two failure modes existing in the joint.

The double-lap bolted joint includes two middle plates jointed through two connecting plates, as shown in Figure 1. The middle and connecting plates of the joint were made of a 3.175 mm thickness Al alloy 7075-T6 plate. The surfaces of the plates were polished to obtain a smooth surface. The plates were joined together using two high strength steel bolts (M5 × 0.8-30, grade 8.8) by applying tightening torque to the bolts using a Norbar torque wrench. The tightening torque can develop an identical clamping force at the joint. Three different tightening torques of $T = 2, 5, \text{ and } 8 \text{ N m}$ were

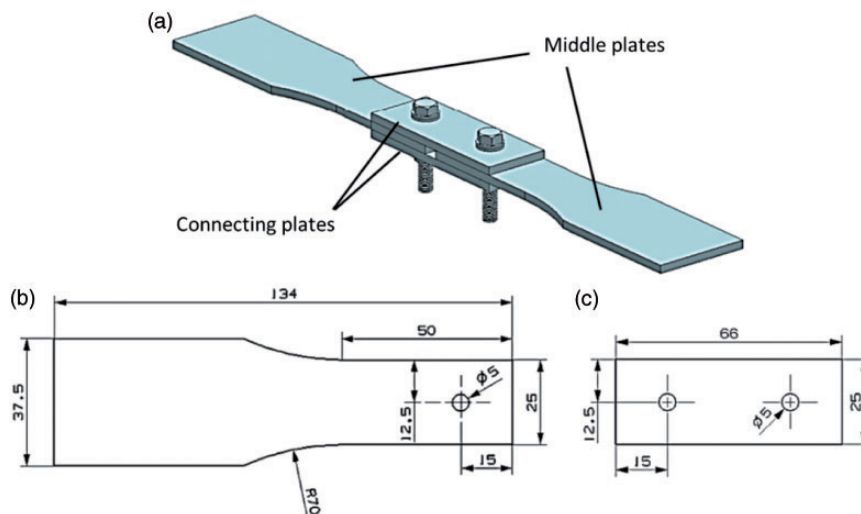


Figure 1. Double-lap bolted joint: (a) joint assembly, (b) middle plate, and (c) connecting plate, dimensions in mm (Oskouei and Ibrahim, 2012).

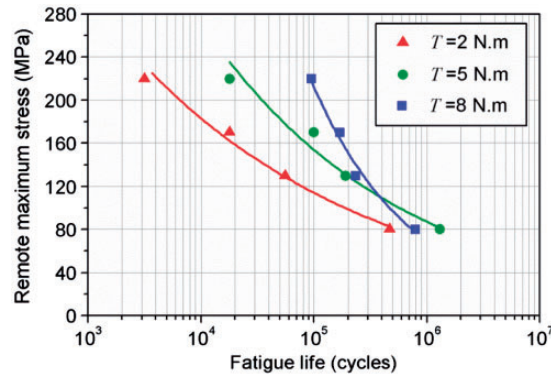


Figure 2. Stress–life curves for Al 7075-T6 bolted joints clamped with different tightening torques (Oskouei and Ibrahim, 2012).

selected to clamp the joint, which create clamping forces equal to $F_{cl} = 976, 2440, \text{ and } 3904 \text{ N}$, respectively, according to the experimental tests (Oskouei and Chakherlou, 2009). Fatigue tests were performed under the constant-amplitude cyclic loading at a frequency of 10 Hz with a load ratio of 0.1. For each batch of specimens, the tests were performed at different levels of remote maximum cyclic stress (S_{max}). The maximum cyclic stress in the cross-sectional area was determined as 80, 130, 170, and 220 MPa to obtain fatigue tests results in both low and relatively high cycle fatigue zones of the joints. A minimum of two fatigue tests was used for each batch at each level of cyclic load.

For the purpose of providing a clear understanding of the two different failure modes under different loading conditions, the authors briefly introduce the main conclusion given by Oskouei and Ibrahim (2012). Figure 2 shows the $S-N$ curves of bolted joints clamped with different tightening torques. The higher clamping force is shown to produce a significant increase in the fatigue life of the bolted joints at high cyclic stress. However, the joints clamped with $T = 8 \text{ N m}$ show a reduction in the fatigue life compared to the joints clamped with $T = 5 \text{ N m}$ at low cyclic stress of 80 MPa. Figure 3 (Oskouei and Ibrahim, 2012) shows the fractured middle plate of the bolted joints at different cyclic loads. On the one hand, wear scar was found near the hole at the 5 and 8 N m bolted joints (Figure 3(a) and (b)) under high cyclic loading due to the gross sliding of the plate surface which can generally increase the fatigue life by removing the damaged material. In these cases, fatigue cracks initiate from the edge of the hole due to the high stress concentration instead of initiating at the contact surface. On the other hand, fretting fatigue failure was found to occur on the contact surface of the bolted joints (Figure 3(c) and (d)) clamped with 5 and 8 N m at low cyclic stress of 80 MPa. The fretting cracks were obviously shown initiating from the contact surface away from the hole. It is also found that fretting was more pronounced in the bolted joints clamped with 8 N m as a result of the higher contact force introduced between the plates. Moreover, there is no significant fretting damage found in the bolted joints clamped with torque of 2 N m. In that case the joints failed from the hole edge due to the stress concentration. Oskouei and Ibrahim (2012) conducted the above experiment and explained the result qualitatively but did not propose quantitative method to explain the effect of clamping force on fatigue and fretting failure. However, the present study attempts to analyze those two failure modes numerically and to present some characteristic of damage evolution in the failure process of the bolted joint quantitatively.

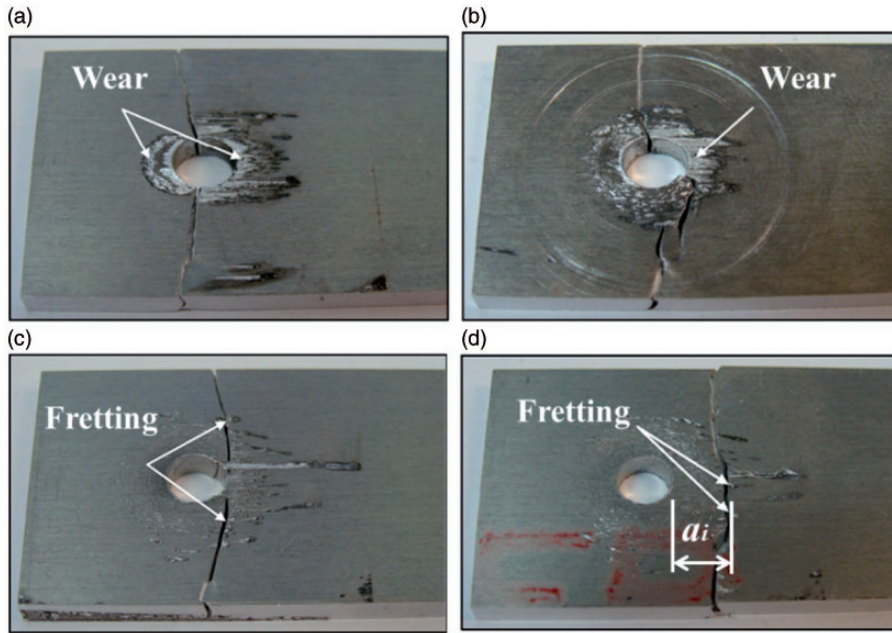


Figure 3. Fractured middle plate of the bolted joints under maximum cyclic stress of 80 and 220 MPa with tightening torques of 5 and 8 N m (Oskouei and Ibrahim, 2012). (a) $T = 5$ N m, $S_{\max} = 220$ MPa, (b) $T = 8$ N m, $S_{\max} = 220$ MPa, (c) $T = 5$ N m, $S_{\max} = 80$ MPa, (d) $T = 8$ N m, $S_{\max} = 80$ MPa.

Theoretical models

Due to the different damage mechanism between fatigue damage and fretting fatigue damage, different fatigue models are used to describe the fatigue and fretting damage evolution. The stress-based and plastic-strain-based models are used to calculate the fatigue damage of material, while a fretting damage criterion in conjunction with a fretting damage model is used to predict the fretting fatigue failure on the contact surface. According to the studies (Szolwinski and Farris, 1998), a large portion of fatigue life is spent in crack initiation (between 85 and 90%). Therefore, the crack initiation life is approximately considered as the total life to failure.

Damage-coupled Chaboche plasticity constitutive model

The damage-coupled plasticity constitutive model proposed by Lemaitre and Chaboche (1990) is used to model the behavior of a damaged and hardened plastic material.

A representative volume element (RVE) is introduced to describe the deterioration of the material under external loading. The properties of the RVE are represented by the homogenized variables. The typical dimension of an RVE is near 0.1 mm for metals. In this study, it is assumed that damage is isotropic and can be represented by the decrease in the elastic modulus (Lemaitre and Chaboche, 1990). The damage variable is thus defined as follows

$$D = 1 - \tilde{E}/E_0 \quad (1)$$

where \tilde{E} is the equivalent elastic modulus of the damaged RVE, and E_0 is the initial elastic modulus of the material.

Considering a small deformation, the total strain ε_{ij} can be decomposed as

$$\varepsilon_{ij} = \varepsilon_{ij}^e + \varepsilon_{ij}^p \quad (2)$$

where ε_{ij}^e and ε_{ij}^p are the elastic and plastic strains, respectively. According to the principle of strain equivalence, the elastic strain takes the form

$$\varepsilon_{ij}^e = \frac{1+\nu}{E_0} \frac{\sigma_{ij}}{1-D} - \frac{\nu}{E_0} \frac{\sigma_{kk}}{1-D} \delta_{ij} \quad (3)$$

where ν is Poisson's ratio, σ_{ij} is the Cauchy stress, and δ_{ij} is the Kronecker delta. The nonlinear kinematic hardening model (NLKH) proposed by Chaboche (1991) is used to represent the kinematic hardening behavior. The von Mises yield function is expressed by

$$f = \sqrt{\frac{3}{2} \left(\frac{s_{ij}}{1-D} - \alpha_{ij} \right) \left(\frac{s_{ij}}{1-D} - \alpha_{ij} \right)} - Q \quad \text{where } \alpha_{ij} = \sum_{k=1}^M \alpha_{ij}^{(k)} \quad (4)$$

where s_{ij} is the deviatoric part of the stress, α_{ij} is the deviatoric part of the back stress, and Q is the radius of the yield surface and its evolution is defined as

$$\dot{Q} = \dot{\lambda} b (Q_\infty - Q) \quad (5)$$

where b and Q_∞ are material constants, $\dot{\lambda}$ is the plastic multiplier that is determined by the plastic flow consistency condition: $\dot{f} = f = 0$. The evolution of the plastic strain components (Lemaitre and Chaboche, 1990) can be obtained as

$$\dot{\varepsilon}_{ij}^p = \frac{3}{2} \frac{\dot{\lambda}}{1-D} \left(\frac{s_{ij}}{1-D} - \alpha_{ij} \right) / \left(\frac{s_{ij}}{1-D} - \alpha_{ij} \right)_{eqv} \quad (6)$$

$$\dot{p} = \sqrt{\frac{2}{3}} \dot{\varepsilon}_{ij}^p \dot{\varepsilon}_{ij}^p = \frac{\dot{\lambda}}{1-D} \quad (7)$$

$$\dot{\alpha}_{ij}^{(k)} = \left(\frac{2}{3} C_k \dot{\varepsilon}_{ij}^p - \gamma_k \alpha_{ij}^{(k)} \dot{p} \right) (1-D) \quad (8)$$

where \dot{p} is the accumulated plastic strain rate. In equation (8), C_k and γ_k are material constants that are determined from experimental tests.

Fatigue damage evolution models

Based on the low-cycle fatigue tests performed by Kang et al. (2009), the damage D can be considered to occur in two parts: elasticity- and plasticity-related damage, which are dependent on the cyclic stress and accumulated plastic strain, respectively. Thus

$$D = D_e + D_p \quad (9)$$

The evolution law (Lemaitre, 1985) of the plasticity damage D_p is given by

$$\dot{D}_p = \left(\frac{\sigma_{eqv}^2 R_v}{2E_0 S (1 - D_p)^2} \right)^m \dot{p} \quad (10)$$

$$R_v = \frac{2}{3}(1 + \nu) + 3(1 - 2\nu)(\sigma_H / \sigma_{eqv})^2 \quad (11)$$

where S and m are material parameters, R_v is the stress triaxiality function, and σ_H and σ_{eqv} are the hydrostatic and von Mises stresses, respectively.

The evolution law of the elasticity damage has been described by Lemaitre and Chaboche (1990). For the multiaxial cyclic loading, the damage rate equation of the nonlinear continuous damage model (NLCD) can be written as

$$\dot{D}_e = \frac{dD}{dN} = [1 - (1 - D)^{\beta+1}]^\alpha \cdot \left[\frac{A_{II}}{M_0(1 - 3b_2\sigma_{H,mean})(1 - D)} \right]^\beta \quad (12)$$

where N is the number of cycles until failure; α , β , M_0 , and b_2 are material constants that are determined by fatigue tests. In equation (12), A_{II} and $\sigma_{H,mean}$ are the amplitude of an octahedral shear stress and the mean hydrostatic stress, respectively

$$A_{II} = \frac{1}{2} \left[\frac{3}{2} (S_{ij,max} - S_{ij,min}) \cdot (S_{ij,max} - S_{ij,min}) \right]^{1/2} \quad (13)$$

$$\sigma_{H,mean} = \frac{1}{2} (\sigma_{H,max} + \sigma_{H,min}) \quad (14)$$

where $S_{ij,max}$ and $S_{ij,min}$ are the maximum and minimum values of the deviatoric stress tensor ij components during one loading cycle, while $\sigma_{H,max}$ and $\sigma_{H,min}$ are the maximum and minimum hydrostatic stresses during one loading cycle. Also in equation (12), the parameter α is given by

$$\alpha = 1 - a \left\langle \frac{A_{II} - A_{II}^*}{\sigma_u - \sigma_{eqv,max}} \right\rangle \quad \text{where} \quad A_{II}^* = \sigma_{I0} (1 - 3b_1\sigma_{H,mean}) \quad (15)$$

where $\sigma_{eqv,max}$ is the maximum von Mises stress during one loading cycle, σ_{I0} is the fatigue limit at zero mean stress, and b_1 is a material constant. The number of cycles until failure is given by integrating equation (12) between $D = 0$ and $D = 1$

$$N_F = \frac{1}{1 + \beta} \cdot \frac{1}{aM_0^\beta} \cdot \frac{\langle \sigma_u - \sigma_{eqv,max} \rangle}{\langle A_{II} - A_{II}^* \rangle} \cdot \left[\frac{A_{II}}{1 - 3b_2\sigma_{H,mean}} \right]^{-\beta} \quad (16)$$

Fretting fatigue damage model

Ferjaoui et al. (2015) and Hojjati-Talemi et al. (2014) developed a CDM approach in conjunction with fretting damage parameter to predict fretting fatigue life. First, the fretting damage parameter

is used to find the location of initial crack at the contact interface by finite element analysis. Second, the CDM model is used to estimate the fatigue life at the location of crack initiation.

According to the study performed by Ruiz et al. (1984), the primary surface damage driving factors are related to the relative slip amplitude δ , shear stress τ , and maximum stress σ_{\tan} in tangential direction at the contact interface. Accordingly, the fretting damage parameter κ is expressed as

$$\kappa = \tau \cdot \delta \cdot \sigma_{\tan} \quad (17)$$

The fretting fatigue crack is considered to initiate from the location of maximum value of κ at the contact interface.

The evolution law (Hojjati-Talemi et al., 2014) of the fretting fatigue damage is expressed as

$$\dot{D} = \frac{2}{C^{\chi/2}(2E)^{\chi/2+1}} \cdot \frac{\sigma_{eqv}^{\chi+1} R_v^{\chi/2+1}}{(1-D)^{\chi+2} \sigma_{eqv}} \quad (18)$$

where C and χ are material constants. The variations of the triaxiality ratio $R_v = \sigma_H/\sigma_{eqv}$ and $(1-D)$ within one cycle are assumed negligible. The derivation of equation (18) over one cycle is then obtained

$$\begin{aligned} \frac{\partial D}{\partial N} &= \int_{t_1}^{t_2} \dot{D} dt = G \frac{\sigma_{eqv, \max}^{\chi+2} - \sigma_{eqv, \min}^{\chi+2}}{(1-D)^{\chi+2}} R_v^{\chi/2+1} \\ G &= \frac{2}{C^{\chi/2}(\chi+2)(2E)^{\chi/2+1}} \end{aligned} \quad (19)$$

The damage variable D can be written as a function of number of cycles by integrating equation (19) between $D = 0$ and $D = 1$

$$N_F = \frac{1}{G \cdot (\chi + 3)} \left(\sigma_{eqv, \max}^{\chi+2} - \sigma_{eqv, \min}^{\chi+2} \right)^{-1} R_v^{-\chi/2-1} \quad (20)$$

It is worth noting that the above fretting fatigue model is a stress-based model, which is for the case of elastic damage. It is reasonable to use this model here since only elastic deformations occur at the fretting area. This is because the contact area is relatively away from the hole edge. Thus, in the analysis of fretting fatigue the elasto-plastic damage evolution need not be considered.

Identification of material parameters

Three groups of material parameters in fatigue damage models are needed to be identified based on the experimental data from uniaxial tensile tests, low-cycle and high-cycle fatigue tests. The experimental data are obtained from the Dowling (1993) and MIL-HDBK-5H handbook (1998). For the parameters in fretting fatigue damage, they are identified from the test data of bolted joint. The best least square fit is used to determine the parameters. The methodology and results are briefly introduced below.

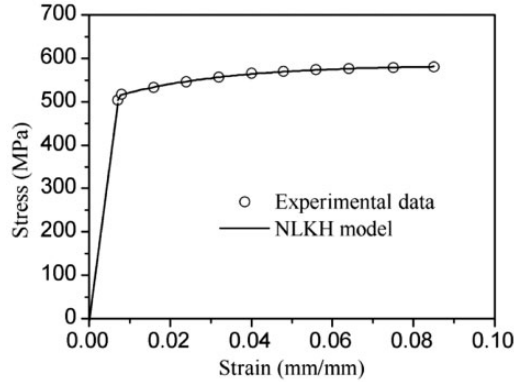


Figure 4. Stress–strain curve for Al alloy 7075-T6.

Table 1. Static mechanical and material parameters for Al alloy 7075-T6.

E (MPa)	ν	σ_y (MPa)	σ_u (MPa)	C_1 (MPa)	C_2 (MPa)	C_3 (MPa)	γ_1	γ_2	γ_3
71,500	0.33	503	600	784.3	1743.2	126,767.4	34.5	34.7	11,840

Identification of material parameters in the plasticity constitutive equations. The parameters in the constitutive equations are determined by the stress–strain curve obtained from the uniaxial tensile test. Three components of the back stress ($M = 3$) are used to represent the NLKH behavior. The isotropic hardening is neglected in this study. The stress–strain curve is expressed as follows

$$\sigma = \sigma_y + \sum_{k=1}^M \frac{C_k}{\gamma_k} (1 - e^{-\gamma_k \varepsilon_p}) \quad (21)$$

where σ_y and ε_p are the initial yield stress and the plastic strain, respectively. Figure 4 shows the fitting curve of the stress–strain curve, and the parameters are summarized in Table 1.

Identification of material parameters in the fatigue damage evolution models. The parameters m and S in the evolution law of the plasticity damage are determined from the strain-controlled low-cycle fatigue test data. Based on the Coffin–Manson relationship, the strain–life curve can be written as follows

$$\frac{\Delta \varepsilon_p}{2} = \varepsilon'_f (2N_F)^c \quad (22)$$

where ε'_f and c are material parameters. Using the cyclic stress–strain curve described by

$$\sigma_{\max} = H' (\Delta \varepsilon_p / 2)^{n'} \quad (23)$$

where H' and n' are material parameters.

From the fatigue damage evolution model presented in equation (10), for the uniaxial case, the number of cycles until failure is obtained by integrating equation (10) from $D = 0$ to D_c

$$N_F = \frac{1 - (1 - D_c)^{2m+1}}{2(2m + 1)} \left(\frac{2^{1+2n'} ES}{H^2} \right)^m (\Delta \varepsilon_p)^{-(1+2mm')} \quad (24)$$

where D_c is the critical value of the damage at macrocrack initiation. The parameter D_c is determined from rapture stress and ultimate stress of a tension test and the details have been described in literature (Lemaitre and Rodrigue, 2005). The values of ε'_f , c , H' , and n' are obtained from low-cycle fatigue tests (Dowling, 1993). The material parameters in equations (10) and (24) are obtained by equating equations (22) and (24) and are shown in Table 2.

The stress–life curve (Dowling, 1993) of unnotched specimens for Al alloy 7075-T6 is used to identify the parameters of the NLCD model. The fatigue limit σ_{f0} and b_1 are obtained from stress–life data at different stress ratios (e.g. $R = -1, 0$, and 0.5). The values of M_0 and β can be determined numerically by stress–life data at stress ratio $R = -1$, and b_2 can be determined from stress–life data at different stress ratios (e.g. $R = 0$ and 0.5). Based on the known values of $\alpha M_0^{-\beta}$ and β , a can be identified numerically. The details of this method have been described by Shen et al. (2015a) and Zhang et al. (2012). The identified material parameters are shown in Table 3. Figure 5 shows the comparison of the integrated NLCD model and experimental data (Dowling, 1993).

Table 2. Material parameters of the plasticity damage model for Al alloy 7075-T6.

S	m	D_c	ε'_f	c	H'	n'
10.45	2.88	0.08	0.262	−0.619	977	0.106

Table 3. Material parameters of the NLCD model for Al alloy 7075-T6.

β	$\alpha M_0^{-\beta}$	b_1	b_2	σ_{f0}	a
3.80	2.243×10^{-15}	0.0015	0.0012	46 MPa	0.70

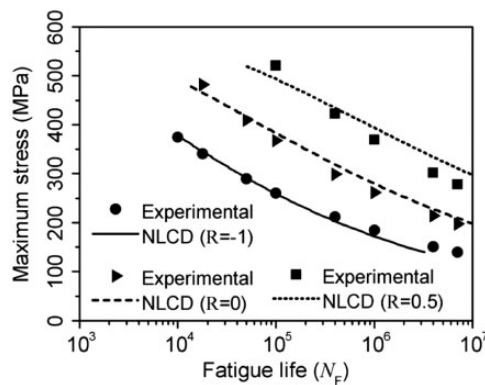


Figure 5. Fatigue life comparison between the integrated NLCD model and experimental data.

Identification of material parameters in the fretting fatigue damage model. In this paper, a small part of the experimental data of double-lap bolted joints (Oskouei and Ibrahim, 2012) is used to identify the fretting damage parameters in equation (20). According to the finite element results in “Finite element analysis” section, the fretting fatigue crack initiation location can be determined based on equation (17), as shown in Table 4. The value of the fretting damage parameters was then determined using best least square fit method based on the finite element results (Table 4) and experimental data. The identified fretting damage parameters are shown in Table 5.

Finite element model and numerical simulation scheme

Finite element model

One-eighth of the specimen is modeled using the ABAQUS software. The model of the joint specimen consists of three sets of elements for the middle plate, connecting plate, and bolt, respectively, as shown in Figure 6. A 3D eight-node linear element (C3D8) is used to mesh the plates and bolt. The meshes around the bolt hole are refined with the minimum mesh size of 0.1 mm. The damage-coupled Chaboche constitutive model is adopted to simulate the stress–strain behavior of Al alloy 7075-T6. While for the bolt, a linear elastic material behavior is used with the elastic modulus of

Table 4. Numerical crack initiation position and von Mises stress.

	Crack location (mm)	$\sigma_{eqv,max}$ (MPa)	$\sigma_{eqv,min}$ (MPa)	R_v
$\sigma_{max} = 80$ MPa, $T = 8$ N m	3.64	128.16	46.97	0.98
$\sigma_{max} = 130$ MPa, $T = 8$ N m	3.21	212.43	65.99	0.97
$\sigma_{max} = 170$ MPa, $T = 8$ N m	2.84	278.96	97.22	0.95

Table 5. Material parameters of the fretting damage model for Al alloy 7075-T6.

G	χ
5.134E-11	-0.1053

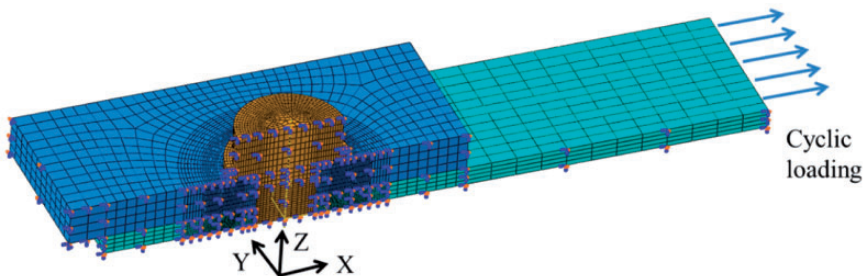


Figure 6. Finite element model of the bolted joint specimen.

207 GPa and Poisson's ratio of 0.3. Symmetric boundary conditions at the three planes of symmetry were used. The contacts between the Al plates and between the bolt and plates are defined using the master–slave algorithm. These contact sets allow the pressure to be perfectly transferred between the contacting surfaces and avoid the contacting areas penetrating each other. For the Al plates pairs, a coefficient of friction $\mu = 0.65$ is used, which is cited from De Pauw et al. (2014) and Hojjati-Talemi et al. (2014). For the coefficients of friction between bolt and Al plates, $\mu = 0.288$ is used (Chakherlou et al., 2008). It should be noted that the algorithm in ABAQUS can ensure simulating correctly the different contact states including sticking, slipping, and detaching. Two primary steps are included in the simulations. In the first load step, the clamping load F_{cl} is applied to the bolt section and then fixed at current length. In the second load step, the cyclic load is applied at the end of the middle plate.

Finite element analysis

As mentioned in the previous section, the fatigue cracks are prone to initiate from the edge of the hole due to the stress concentration, while the fretting cracks usually initiate from the contact surface due to the oscillatory displacements. The final failure mode is influenced by the external loading, while actually is determined by the stress field of the plate. The maximum principal stress σ_1 and shear stress τ are then used to illustrate the influence of clamping force and cyclic stress level on the stress distribution of the plate.

Figure 7 shows the variations of σ_1 and τ at the contact interface of the bolted joint under different levels of cyclic stress with a tightening torque of $T = 8 \text{ N m}$. As shown, the position of maximum principal stress moves from somewhere away from the hole to the edge of the hole with a sharp increase from 132 to 552 MPa as the increase of applied cyclic stress from 80 to 220 MPa. The location of maximum shear stress also moves from the place away from the hole to the hole edge as the cyclic stress increases. The variation of maximum principal stress and shear stress can indicate, to

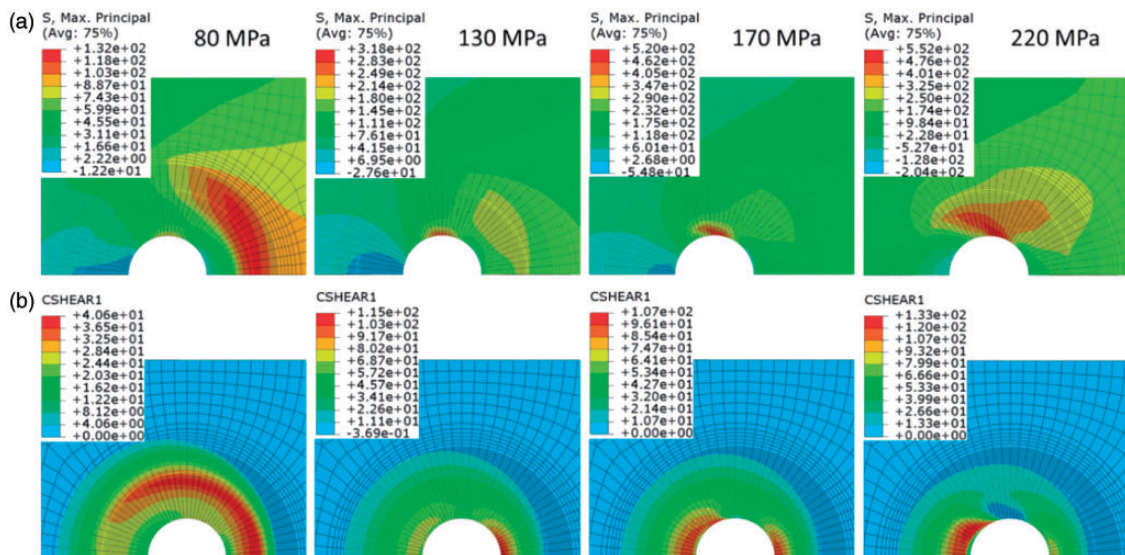


Figure 7. Variations of the maximum principal stress (a) and shear stress (b) at the contact interface.

some extent, the change of failure mode and crack initiation location under different applied cyclic loadings.

Figure 8 shows the variation of contact status for the bolted joints under different cyclic load with a tightening torque of 8 N m. The contact regions can be divided into sticking and slipping regions. For the 80 MPa case, mixed stick–slip areas are shown at both maximum and minimum loads of the cycle. It suggests that the junction of sticking and slipping regions keeps moving during the loading cycle. As the cyclic load levels increase from 80 to 170 MPa, the stick region is significantly decreased. The variations of the contact status are related to the relation between cyclic loading and normal clamping force, because the cyclic loading is directly related to the traction force on the contact surface while the normal clamping force determines the frictional force. The contact status also influences the failure mode.

On the basis of the computational results one can obtain the variations of the relative slip amplitude δ , shear stress τ , fretting damage parameter κ , and von Mises stress σ_{eqv} along a path, from which one may acquire valuable information about the prediction of the fretting damage on the contact surface. Figure 9 shows the variation of these qualities along Path-2 marked in Figure 8. It is shown from Figure 9(a) that as the load increases from 80 to 220 MPa, δ continually increases which indicates slipping condition changing from partial slip to a gross slip. As shown in Figure 9(b), the maximum τ is located at the position with a distance of 2 mm away from the hole edge for the 80 MPa case. It is also noted that as the load increases from 80 to 220 MPa, the location of the maximum τ moves to the hole edge and the value of which increases first and then decreases. The maximum value of κ (Figure 9(c)) is shown to significantly increase as the load increases. The location of maximum κ becomes closer to the hole edge with the increase of the cyclic load. Moreover, it is found that there is no significant stress concentration on the contact surface due to the smooth contact between the plates. The distribution of σ_{eqv} shown in Figure 9(d) demonstrates that point.

Numerical simulation scheme

In this paper, the fatigue damage and fretting fatigue damage are simulated separately. The fatigue life is calculated at each integration point of the material element, while the fretting fatigue life is

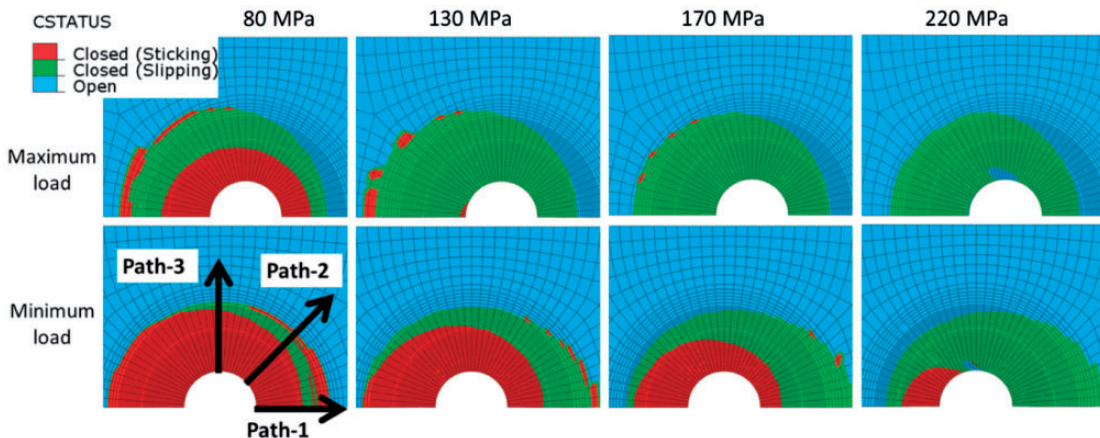


Figure 8. Variations of the contact status for the bolted joints under different cyclic loads.

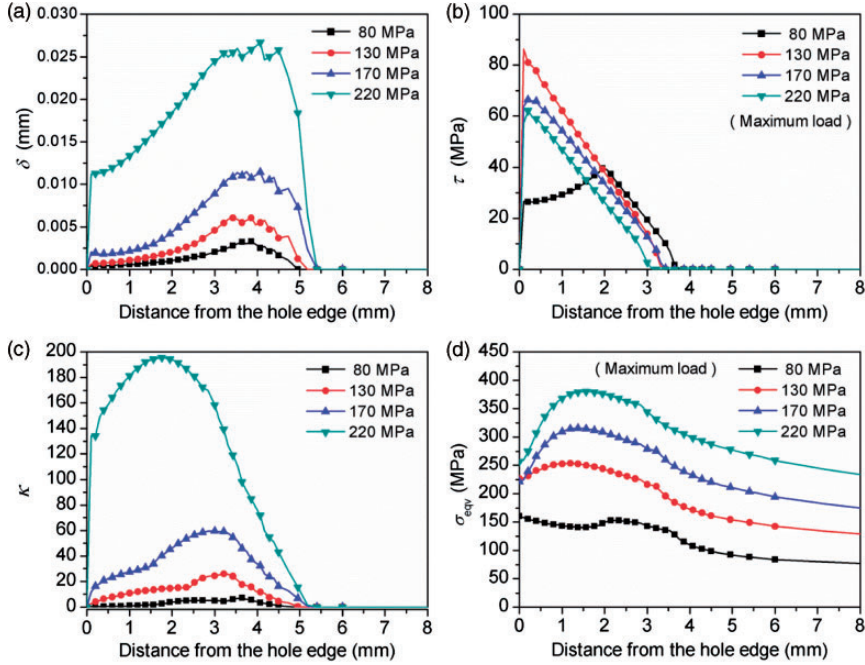


Figure 9. Variations of relative slip amplitude (a), shear stress (b), fretting damage parameter (c), and von Mises stress (d) over the contact line Path-2.

computed just on the contact surface of the plate. The predicted cycles to failure are considered to be the smaller one of the fatigue life and fretting fatigue life

$$N_F = \text{Min} (N_{\text{fatigue}}, N_{\text{fretting}}) \quad (25)$$

For the fatigue damage simulation, the user material subroutine is used to implement the calculation of the damage-coupled Chaboche plasticity constitutive model and the fatigue damage evolution equations. The subroutine updates the stress and solution-dependent variables and the Jacobian matrix at each time increment, and calculate the accumulated damage at each integration point during the cycles. A cycle jumping factor ΔN is used to reasonably save the amounts of computational time. It is assumed that the stresses, the increment of accumulated plastic strain, and the increment of damage are the same for each cycle during each block of ΔN cycles. According to the study carried out by Shen et al. (2015a) and Zhang et al. (2012), a convergent result can be obtained when $\Delta N/N_F < 0.02$, which is also verified in the paper. The simplified algorithm is shown in Figure 10. The details of the numerical simulation scheme are listed as follows:

- (1) The clamping force is applied in the bolt by bolt pretension method using ABAQUS.
- (2) The cyclic stress and the accumulated plastic strain are calculated under cyclic loading.
- (3) The fatigue damage is calculated based on equations (10) and (12) after ΔN cycles, the accumulated damage given as

$$D^{(i+1)} = D^{(i)} + \Delta N \cdot \dot{D}_e^{(i+1)} + \Delta D_p^{(i+1)} \quad (26)$$

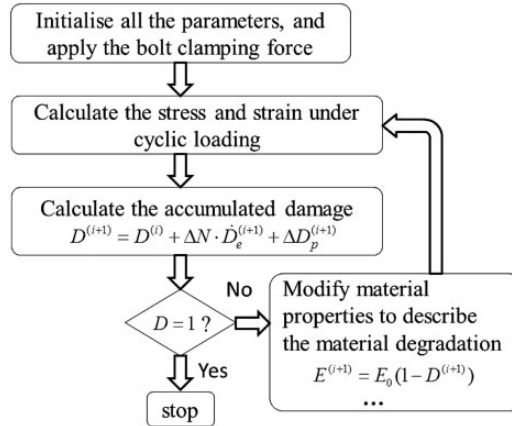


Figure 10. Simplified algorithm of the numerical simulation.

$\Delta D_p^{(i+1)}$ is dependent on whether cyclic plasticity occurred during the ΔN cycles

$$\Delta D_p^{(i+1)} = \begin{cases} \Delta N \cdot \dot{D}_p^{(i+1)} & \text{cyclic plasticity} \\ \dot{D}_p^{(i+1)} & \text{else} \end{cases} \quad (27)$$

(4) The material properties of the damaged element are modified to account for the material degradation

$$E^{(i+1)} = E^{(i)}(1 - D^{(i+1)}) \quad (28)$$

$$C_k^{(i+1)} = C_k^{(i)}(1 - D^{(i+1)}) \quad (29)$$

$$\gamma_k^{(i+1)} = \gamma_k^{(i)}(1 - D^{(i+1)}) \quad (30)$$

(5) The algorithm repeats steps (2)–(4) until the damage of any integration points reaches a value of 1, which indicates that a fatigue crack initiation has begun to form.

For the fretting fatigue life prediction, the Ruiz criterion (equation (17)) is used to locate the critical position where the material suffers the most serious fretting damage, then the integrated fretting damage model (equation (20)) is used to calculate the fretting fatigue life.

It is worth noting that in the fatigue damage analysis the calculated damage variable at one material integration point is directly used to predict the crack initiation life, rather than applying the critical averaging dimension approach discussed by Araújo and Nowell (2002), and used by Ding et al. (2014) and Zhu et al. (2013). The reason is that the stress gradient is not severe in this case and the redistribution of the stress induced by the coupled approach also reduces the stress gradient. Therefore, the proposed approach is applicable for this study.

Table 6. Predicted fatigue life for bolted joints clamped with different tightening torques.

		Predicted fatigue life	Predicted fretting fatigue life	Cycles to failure	Failure mode and crack initiation location
2 N m	80	2.56×10^5	1.02×10^6	2.56×10^5	Fatigue, hole-90°
	130	3.10×10^4	1.17×10^6	3.10×10^4	Fatigue, hole-90°
	170	1.08×10^4	1.24×10^6	1.08×10^4	Fatigue, hole-90°
	220	3.18×10^3	3.37×10^6	3.18×10^3	Fatigue, hole-100°
5 N m	80	$>1.0 \times 10^7$	9.65×10^5	9.65×10^5	Fretting-45°, $a_i = 3.2$ mm
	130	8.80×10^5	2.96×10^5	2.96×10^5	Fretting-45°, $a_i = 2.0$ mm
	170	5.45×10^4	2.06×10^5	5.45×10^4	Fatigue, hole-90°
	220	1.12×10^4	3.85×10^5	1.12×10^4	Fatigue, hole-90°
8 N m	80	$>1.0 \times 10^7$	8.18×10^5	8.18×10^5	Fretting-45°, $a_i = 3.6$ mm
	130	$>1.0 \times 10^7$	3.03×10^5	3.03×10^5	Fretting-45°, $a_i = 3.2$ mm
	170	1.82×10^6	1.90×10^5	1.90×10^5	Fretting-45°, $a_i = 3.0$ mm
	220	6.18×10^4	2.72×10^5	6.18×10^4	Fatigue, hole-90°

Results and discussions

Predicted fatigue life and crack initiation site

The fatigue life is calculated by the numerical scheme described in Figure 10; while the fretting fatigue life is calculated using the integrated fretting damage model (equation (20)) combined with the Ruiz criterion (equation (17)).

Table 6 shows the predicted fatigue life and fretting fatigue life for the bolted joint with tightening torques of 2, 5, and 8 N m, respectively. Under the torque of 2 N m all of the joints are predicted to suffer from fatigue failure rather than fretting failure. The bolted joints with the torque of 5 N m are predicted to be fretting failure when the cyclic loadings are 80 and 130 MPa, but fatigue failure when they are 170 and 220 MPa. The bolted joints under torque of 8 N m are predicted to be fretting failure for the cyclic loadings of 80, 130, and 170 MPa cases, but fatigue failure for the 220 MPa case. Three of the 8 N m bolted joints have been used to identify the fretting fatigue parameters. The results are illustrated for comparison purpose. Figure 11 shows the predicted lives versus the experimental results (Oskouei and Ibrahim, 2012) for the bolted joints clamped with different tightening torques. It is shown that the predicted results are located within the twice-error band.

Figure 12 shows the predicted fatigue damage field and crack initiation sites for the bolted joints with different tightening torques under a cyclic loading of 220 MPa. For all the cases the predicted crack is shown to initiate at the hole edge with about 90° from the X-axis. One can see that under the torque of 2 N m the fatigue is of low cycle fatigue and the reason is because the slight tightening torque combined with heavy cyclic loading induces plasticity deformation at the edge of the hole. When the torque increases, the fatigue life becomes longer and longer, which indicates that the greater tightening torque reduces the stress level at the edge of the hole.

Figure 13 shows the cyclic stress–strain curves at the crack initiation location of the bolted joints under cyclic loading of 220 MPa with tightening torques of 2 and 8 N m. In the 2 N m case (Figure 13(a)), significant plastic strain and stress–strain hysteresis loops occur during the first cycle, then the ratcheting stress increases gradually after certain cycles due to cyclic hardening. In

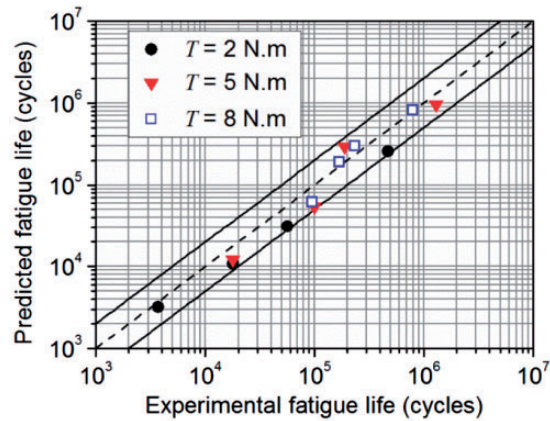


Figure 11. Comparison of the experimental and predicted fatigue lives for the bolted joints (the results are located within the twice-error band).

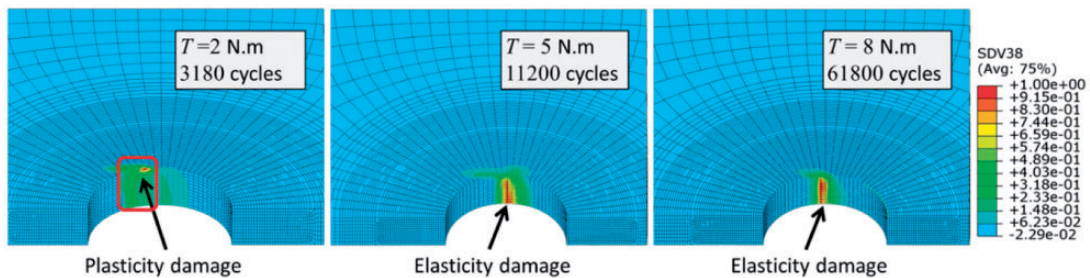


Figure 12. Predicted fatigue damage for the bolted joints under cyclic stress of 220 MPa with different tightening torques.

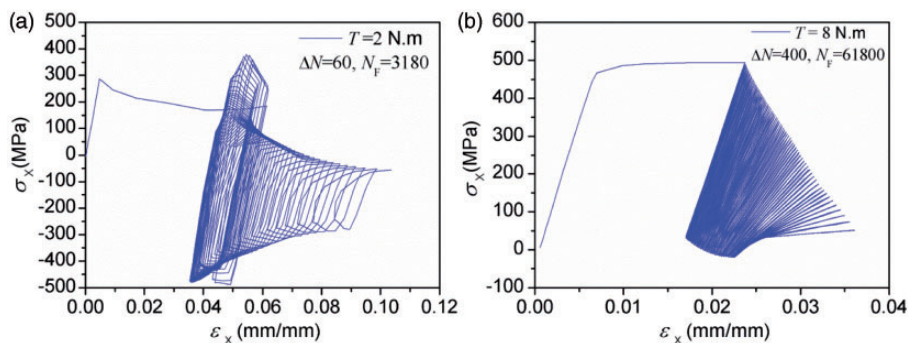


Figure 13. Cyclic stress–strain curves of integration points at crack initiation location for the bolted joints under cyclic stress of 220 MPa. (a) $T = 2$ N m, (b) $T = 8$ N m.

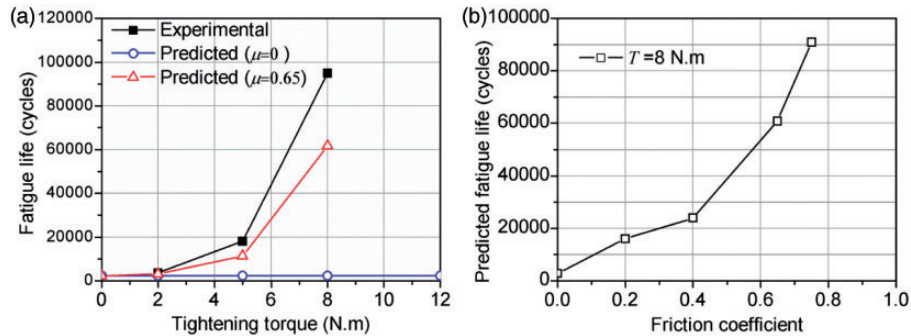


Figure 14. (a) Predicted and experimental fatigue lives versus tightening torque and coefficient of friction, (b) predicted lives versus coefficient of friction.

the last phase, the ratcheting strain increases gradually and stress–strain hysteresis loops become smaller and smaller due to the accumulated plasticity fatigue damage and stress redistribution. For the 8 N m case (Figure 13(b)), plastic strain occurs during the first cycle, while almost no stress–strain hysteresis loops appear till failure. The maximum stress is shown to decrease as the number of loading cycles increases, which can be attributed to the stress redistribution due to the accumulated elasticity damage.

The combined effect of clamping force and coefficient of friction on fatigue damage

As shown in the S – N curves (Figure 2), the bolted joint with tightening torque of 8 N m has a 26 times fatigue life improvement than that of 2 N m case under cyclic loading of 220 MPa. Therefore, Oskouei and Ibrahim (2012) concluded that the fatigue life improvement of the bolted joints is the result of compressive stress around the hole. To investigate this conclusion in detail, the isolated effect of clamping force on fatigue life is investigated. Figure 14 shows the predicted and experimental fatigue lives versus tightening torque for the bolted joint under cyclic stress of 220 MPa with the coefficient of friction $\mu = 0$ and 0.65, respectively. For the $\mu = 0$ case, the predicted fatigue lives show negligible increase with the increase of tightening torque, which means the clamping force itself has very limited benefit on the fatigue life improvement. While for the $\mu = 0.65$ case, the predicted fatigue lives show an obvious increase as the tightening torque increases from 0 to 8 N m. The predicted results for the $\mu = 0.65$ case are shown to be in good agreement with the experimental data (Oskouei and Ibrahim, 2012). Figure 14(b) shows the predicted fatigue life versus friction coefficient for the bolted joint under a cyclic stress of 220 MPa with a tightening torque of 8 N m. It is shown that the fatigue life increases from 2200 to 91,000 cycles as the coefficient of friction increases from 0 to 0.75. Therefore, it can be concluded that the coefficient of friction and clamping force are equally important to the fatigue life improvement, and the greater friction combined with larger clamping force may provide much more benefit. The following process will continue to analyze the mechanism of this improvement.

Figure 15(a) shows the longitudinal stress σ_x at the critical location for the bolted joint with a torque of 8 N m under a cyclic loading of 220 MPa at different coefficients of friction. The stress amplitudes are shown to be significantly decreased when the coefficient of friction increases from 0 to 0.75, but the maximum stresses show little change. Figure 15(b) shows the total force transmitted by the bolt and frictional shear force for the bolted joints at different coefficients of friction. As it shows, with the increase of the coefficient of friction, the total force transmitted by the frictional

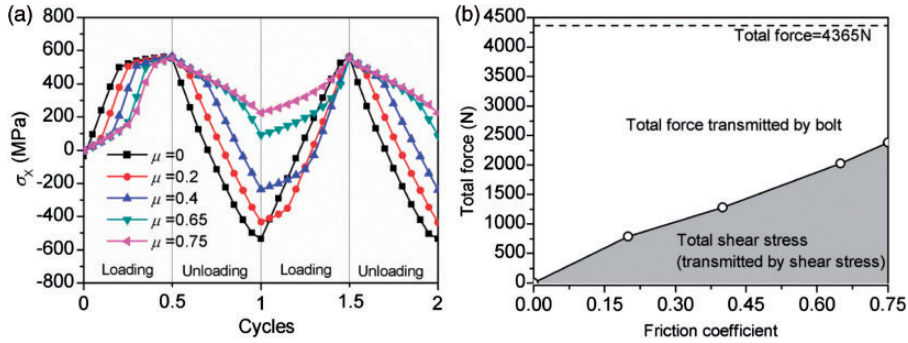


Figure 15. Longitudinal stresses (a) and load transmission (b) for the 8 N m bolted joint under cyclic stress of 220 MPa with different coefficients of friction.

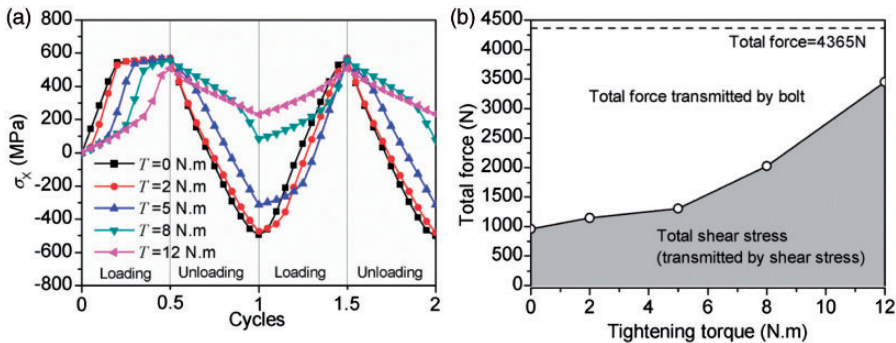


Figure 16. Longitudinal stresses (a) and load transmission (b) for the bolted joint clamped with different tightening torques under cyclic stress of 220 MPa.

force increases and the total force transmitted by the bolt decreases. The decrease in the transmitted load of the bolt will result in the reduction in stress amplitude at the hole edge, which is the essential reason of the fatigue life improvement of the bolted joint.

Figure 16 shows the longitudinal stress σ_x at the critical location for the bolted joint clamped with different tightening torques under a cyclic stress of 220 MPa with a coefficient of friction $\mu = 0.65$. The stress amplitude is shown to have little decrease for the 2 N m case, but shown to have significant decrease as the tightening torque increases from 5 to 12 N m. Figure 18 shows the total force transmitted by bolt and frictional force versus tightening torque for the bolted joints. The load transmitted by the frictional shear stress is shown slightly increased as the tightening torque increases from 0 to 5 N m, and shown significantly increased as the tightening torque increases from 5 to 12 N m. The frictional force that occurred in the 0 N m case resulted from the contact pressure between the plates, which is caused by the high squeezing force between the bolt and hole surface. From the comparison of Figures 15(a) and 16(a), it can be found that the coefficient of friction and clamping force have similar effects on the reduction of stress amplitude for the bolted joint. Therefore, it is concluded that the reduction in stress amplitude is the combined effect of clamping force and frictional force at the contact surface, which is the primary reason of fatigue life improvement.

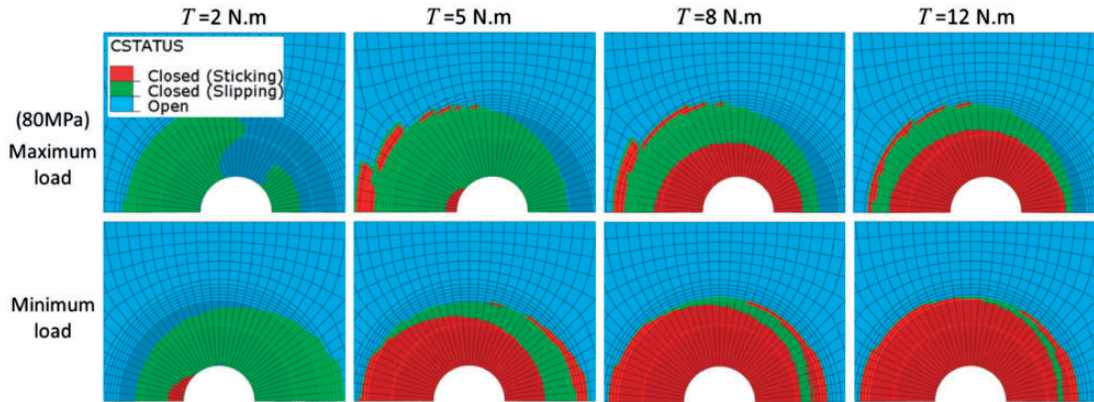


Figure 17. The contact status for the bolted joint under cyclic stress of 80 MPa at different tightening torques.

The effect of clamping force on fretting fatigue damage

As shown in Figure 2, significant fretting fatigue occurs at low stress level and fretting wear occurs at high stress levels in the contact surface of the middle plate. Different fretting damage mode is attributed to the different relative slip amplitude associated with cyclic stress levels. To investigate the clamping force on the fretting damage, the contact conditions for the bolted joints under cyclic loading of 80 and 220 MPa are illustrated. The coefficient of friction is assumed to be 0.65 in this section.

Figure 17 shows the variations of contact status for the bolted joint under cyclic loading of 80 MPa at different tightening torques. The sticking region is shown to increase with the increase of the tightening torque. A mixed stick–slip region is shown to be located at the outside of the hole when the tightening torque increases from 5 to 12 N m. The contact pressure caused by tightening torque is the crucial factor impacting the ratio of slip and stick. When the tightening torque is large enough, the relative movement occurs only in the outside of the hole.

Figure 18 shows the relative slip amplitude δ and fretting damage parameter κ along Path-2 under cyclic loading of 80 MPa. δ is shown decreasing as the tightening torque increases from 2 to 12 N m. For the 2 N m case, a large δ occurs in the contact surface. However, a sharp decrease of δ is shown when the tightening torque increases to 5 N m. As the tightening torque increases to 8 and 12 N m, δ equals to 0 near the hole edge and the maximum value of δ is much reduced compared to the 2 N m case. It is concluded that with the increase of the tightening torque, the contact conditions varying from gross slip condition to mixed stick–slip condition, and position with the maximum fretting damage move away from the hole. The fretting damage parameter is used to find the location of most serious fretting damage, as shown in Figure 18(b). The maximum value of κ is shown to significantly decrease as the tightening torque increases from 2 to 5 N m, and there is no additional decrease as the tightening torque increases from 5 to 12 N m.

Figure 19 shows the variations of the contact status for the bolted joint under cyclic stress of 220 MPa when clamped by different tightening torques. At maximum cyclic load, small contact region is shown in the 2 and 5 N m bolted joints and large slipping region is shown in the 8 and 12 N m bolted joints. At minimum cyclic load, the contact regions are shown enlarged for all of the bolted joints. The significant change in contact regions is related to the Poisson effect. The thickness of the plate will decrease with the increase in tensile cyclic load. The contact status of some regions in

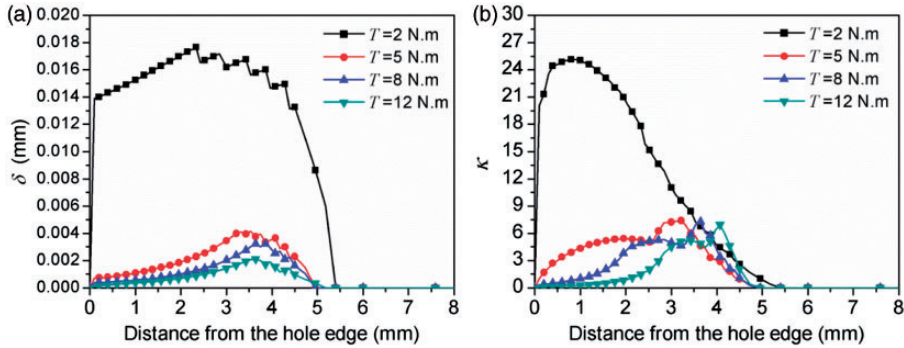


Figure 18. Variations of relative slip amplitude δ (a) and fretting damage parameter κ (b) along the Path-2.

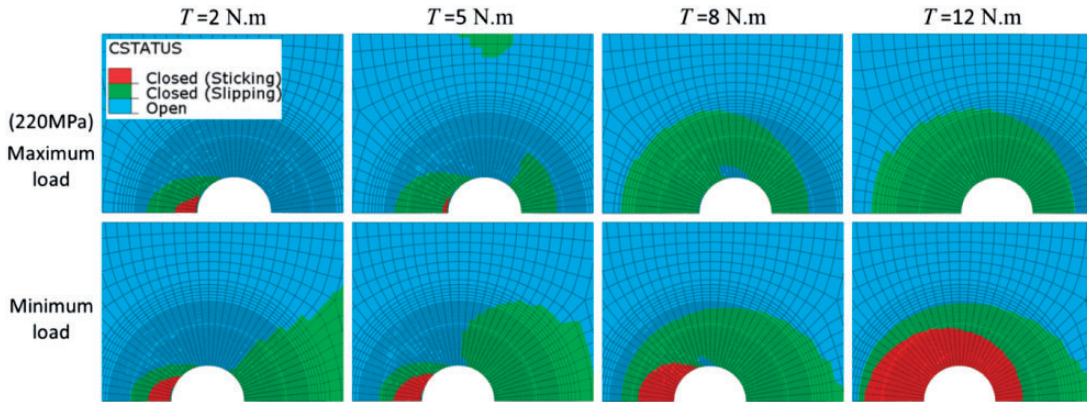


Figure 19. The contact status for the bolted joint under cyclic stress of 220 MPa at different tightening torques.

the plate will be that of open status. Moreover, small sticking regions are shown in the left side of the hole edge, which are caused by the high squeezing force of the bolt on the hole surface and thus the contact pressure is increased between the plates in the sticking regions.

Figure 20 shows the relative slip amplitude δ and fretting damage parameter κ along the Path-2 for the bolted joint under cyclic stress of 220 MPa. For the 2 N m case, little fretting damage occurred due to the transient contact condition during a fatigue cycle. The 2 N m case will not be illustrated. δ is shown to decrease as the tightening torque increases from 5 to 12 N m. For the 5 and 8 N m cases, the maximum value of δ is larger than 0.02 mm indicating a gross slip condition. For the 12 N m cases, δ is shown almost to be 0 near the hole edge, which indicates a mixed stick–slip condition. It is also found that the contact region in the 5 and 8 N m case is in good agreement with the region of fretting wear shown in Figure 2.

In order to illustrate the effect of clamping force on the failure life of the bolted joint, the predicted life N_{fatigue} , N_{fretting} , N_{F} and experimental life N_{EXP} versus tightening torque for the bolted joint under remote stress of 80 and 220 MPa are shown in Figure 21. The lifetime to failure N_{F} is considered to be the smaller one of N_{fatigue} and N_{fretting} . For the 80 MPa case, N_{fatigue} monotonically increases with the increase of the tightening torque, while N_{fretting} monotonically decreases

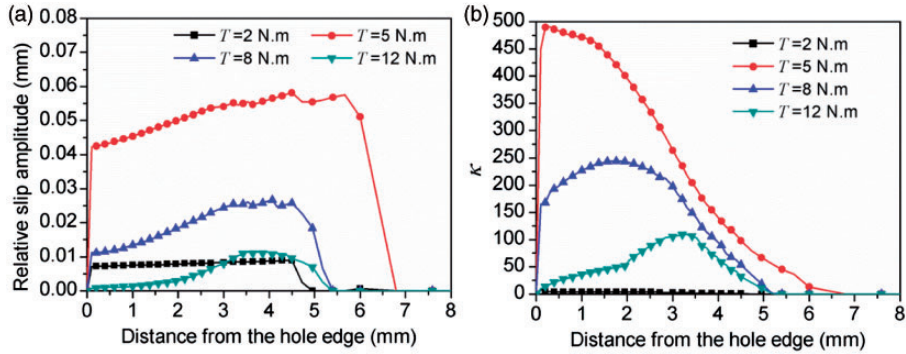


Figure 20. Variations of relative slip amplitude (a), and fretting damage parameter κ (b) over the Path-2.

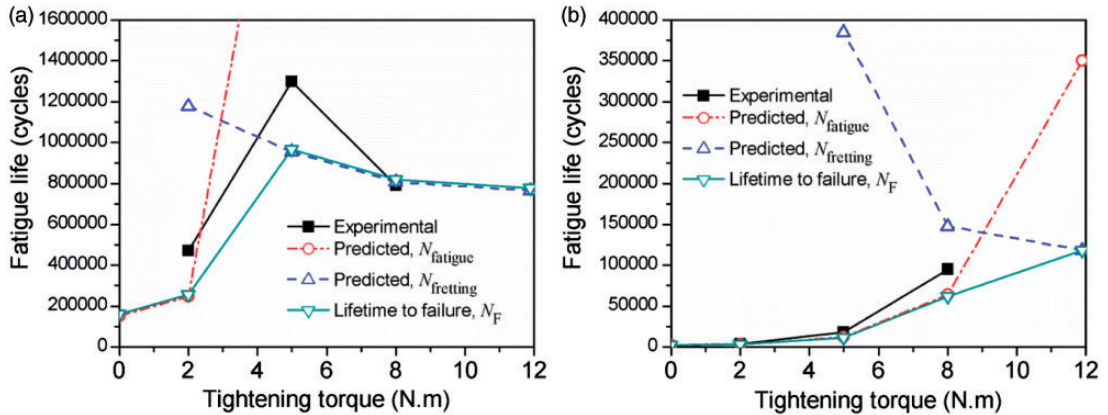


Figure 21. Predicted and experimental fatigue lives versus tightening torque for the bolted joint. (a) 80 MPa, (b) 220 MPa.

with the increase of the tightening torque. The predicted curves of $N_{fatigue}$ and $N_{fretting}$ intersect somewhere. When the tightening torque is smaller than the intersection value a fatigue failure is presented, otherwise a fretting failure is presented. For the 220 MPa case, the predicted $N_{fatigue}$ and $N_{fretting}$ are shown to be similar in trend to the 80 MPa case. The cross point is shown to locate at a high tightening torque of 9 N m when the tightening torque is larger than 9 N m and the failure mode is predicted to be the fretting failure. The predicted N_F for both of the 80 and 220 MPa cases are in good agreement with the experimental results.

The effect of coefficient of friction on fretting fatigue damage

To investigate the effect of the coefficient of friction on fretting damage, the contact status for the bolted joint with tightening torque of 8 N m under cyclic loading of 80 MPa at different coefficient of friction is shown in Figure 22. The surface of the sticking region is shown to increase with the increase of the coefficient of friction. The effect of the coefficient of friction on the contact status is similar to that of the clamping force. Figure 23 shows the variations of the relative slip amplitude

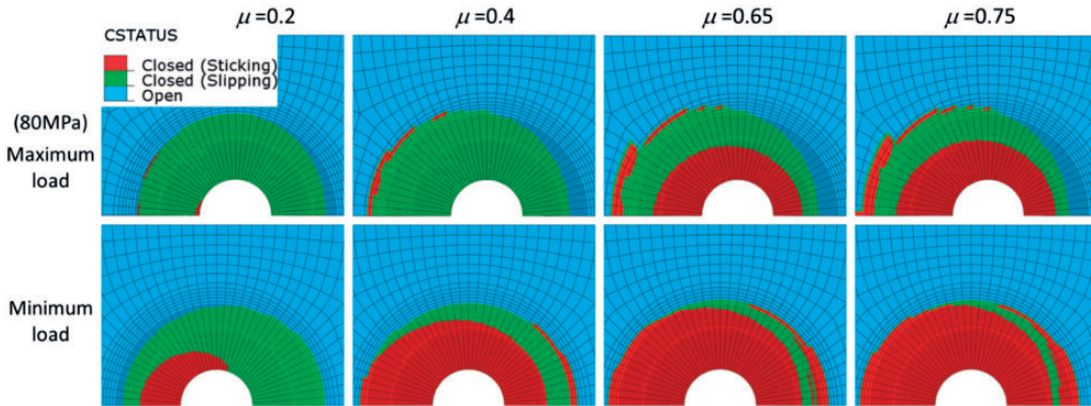


Figure 22. The contact status for the bolted joint under cyclic stress of 80 MPa at different coefficient of friction.

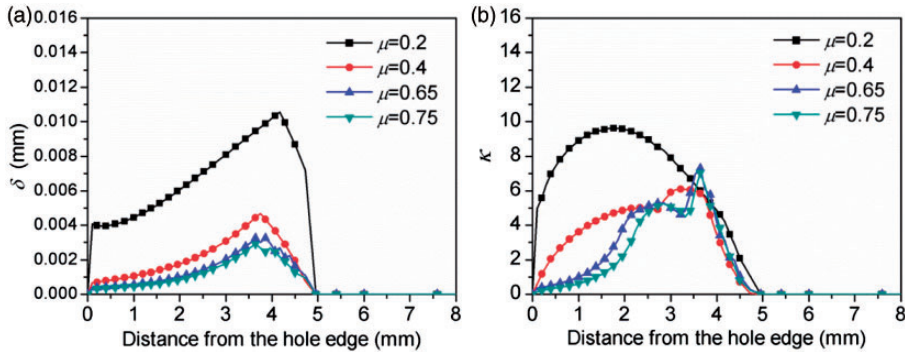


Figure 23. Variations of relative slip amplitude (a), and fretting damage parameter κ (b) over the Path-2 for the bolted joint under cyclic stress of 80 MPa.

δ and fretting damage parameter κ along the Path-2 for the bolted joints. δ decreases when the coefficient of friction increases from 0.2 to 0.65. As the coefficient of friction increases from 0.65 to 0.75, δ is shown to have minor change. For the 0.65 and 0.75 cases, δ almost equals to 0 near the hole edge in the sticking region. It can be concluded that the coefficient of friction influences the fretting damage through inducing the variation of contact status which is the key factor of fretting.

Figure 24 shows the contact status for the 8 N m bolted joint under cyclic stress of 220 MPa with different coefficient of friction. The surfaces of slipping and sticking are shown to increase with the increase of the coefficient of friction. Figure 25 shows the variations of the relative slip amplitude δ and fretting damage parameter κ along the Path-2 for the bolted joints. δ and κ are shown to significantly decrease with the increase of the coefficient of friction.

Figure 26 shows the predicted N_{fatigue} , N_{fretting} , and N_F versus the coefficient of friction for the bolted joint under cyclic stress of 80 and 220 MPa. For the 80 MPa case, N_{fatigue} is shown to increase with the increase of the coefficient of friction from 0 to 0.75, while N_{fretting} is shown to slightly increase with the increase of the coefficient of friction from 0 to 0.4, and then remains approximately constant from 0.4 to 0.75. It can be derived that the fatigue failure mode is predominant when the

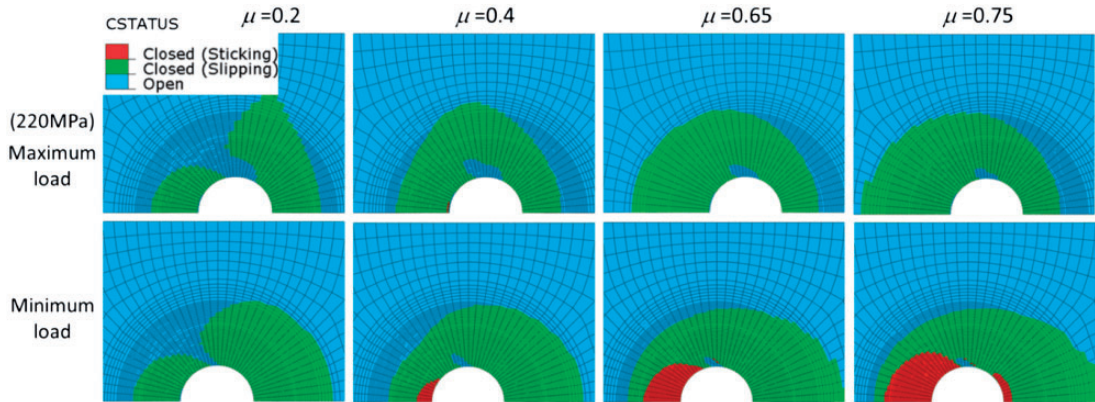


Figure 24. The contact status for the bolted joint under cyclic stress of 220 MPa at different coefficient of friction.

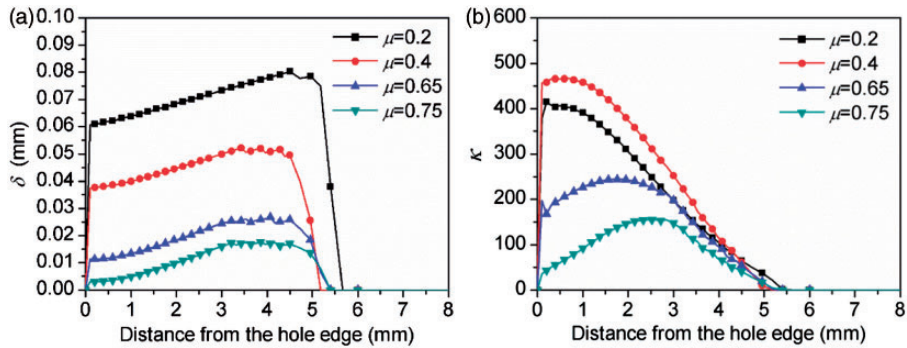


Figure 25. Variations of relative slip amplitude (a), and fretting damage parameter κ (b) over Path-2.

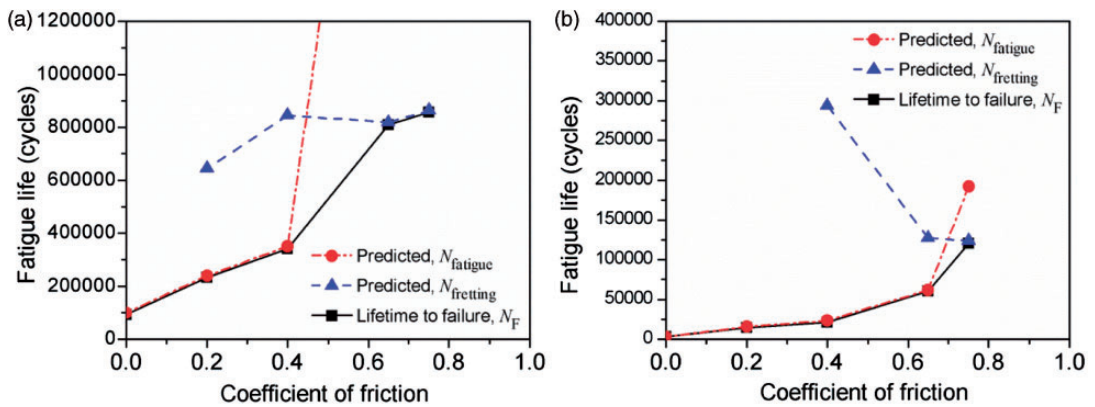


Figure 26. Predicted fatigue lives versus coefficient of friction for the bolted joint. (a) 80 MPa, (b) 220 MPa.

coefficient of friction is smaller than about 0.45, while the fretting failure mode is present when the coefficient of friction is larger than 0.45. For the 220 MPa case, the predicted curves versus coefficient of friction are similar to the curves versus tightening torque. The increasing coefficient of friction is shown to increase the fatigue life and to decrease the fretting fatigue life.

Conclusions

Based on the CDM, the fatigue damage and fretting fatigue damage of double-lap bolted joints are investigated. The damage-coupled Chaboche plasticity constitutive model is used to represent the material behavior. The elastic–plastic fatigue damage evolution equations are adopted to calculate the fatigue damage. Meanwhile the Ruiz Criterion and the fretting fatigue damage model are applied to calculate the fretting fatigue life. The effects of the clamping force on fatigue damage and fretting fatigue damage of the bolted joint are quantitatively investigated. Some key findings are summarized:

- (1) The CDM approach provides an insight into the fatigue damage and fretting fatigue damage of the bolted joint.
- (2) The predicted fatigue and fretting fatigue lives and crack initiation sites of the double-lap bolted joint are in good agreement with experimental results available in the literature.
- (3) The fatigue life improvement of bolted joint is attributed to the combined effect of clamping force and friction force, which reduces the stress amplitude at the critical position.
- (4) The increase of clamping force will increase the fatigue life while decrease the fretting fatigue life at both low-level and high-level cyclic loadings, and the coefficient of friction has the similar effect. The failure mode of the bolted joint is the result of competition between fatigue damage and fretting damage.

Acknowledgments

The authors appreciate very much the support of the Computational Solid Mechanics Laboratory at Louisiana State University.

Declaration of Conflicting Interests

The author(s) declared no potential conflicts of interest with respect to the research, authorship, and/or publication of this article.

Funding

The author(s) received no financial support for the research, authorship, and/or publication of this article.

References

- Araújo JA and Nowell D (2002) The effect of rapidly varying contact stress fields on fretting fatigue. *International Journal of Fatigue* 24: 763–775.
- Chaboche JL (1991) On some modifications of kinematic hardening to improve the description of ratcheting effects. *International Journal of Plasticity* 7: 661–678.
- Chakherlou TN, Oskouei RH and Vogwell J (2008) Experimental and numerical investigation of the effect of clamping force on the fatigue behaviour of bolted plates. *Engineering Failure Analysis* 15(5): 563–574.

- Chakherlou TN, Razavi MJ, Aghdam AB, et al. (2011) An experimental investigation of the bolt clamping force and friction effect on the fatigue behavior of aluminum alloy 2024-T3 double shear lap joint. *Materials and Design* 32: 4641–4649.
- De Pauw J, De Waele W, Hojjati-Talemi R, et al. (2014) On the use of digital image correlation for slip measurement during coupon scale fretting fatigue experiments. *International Journal of Solids and Structures* 51: 3058–3066.
- Ding J, Kang G, Zhu Y, et al. (2014) Finite element analysis on bending fretting fatigue of 316L stainless steel considering ratcheting and cyclic hardening. *International Journal of Mechanical Sciences* 86: 26–33.
- Dowling NE (1993) *Mechanical Behavior of Materials: Engineering Methods for Deformation, Fracture, and Fatigue*. Englewood Cliffs, NJ, US: Prentice-Hall, pp. 719–720.
- Echle R and Voyiadjis GZ (1999) Simulation of damage evolution in a uni-directional titanium matrix composite subjected to high cycle fatigue. *International Journal of Fatigue* 21(9): 909–923.
- Endo K (1981) Practical observations of initiation and propagation of fretting fatigue cracks. In: Waterhouse RB (ed.) *Fretting Fatigue*. London, UK: Applied Science Publishers Ltd., pp. 127–141.
- Endo K, Goto H and Nakamura T (1969) Effects of cycle frequency on fretting fatigue life of carbon steel. *Bulletin of JSME* 12(54): 1300–1308.
- Esmaeili F, Chakherlou TN and Zehsaz M (2014a) Prediction of fatigue life in aircraft double lap bolted joints using several multiaxial fatigue criteria. *Materials and Design* 59: 430–438.
- Esmaeili F, Chakherlou TN and Zehsaz M (2014b) Investigation of bolt clamping force on the fatigue life of double lap simple bolted and hybrid (bolted/bonded) joints via experimental and numerical analysis. *Engineering Failure Analysis* 45: 406–420.
- Ferjaoui A, Yue T, Abdel Wahab M, et al. (2015) Prediction of fretting fatigue crack initiation in double lap bolted joint using continuum damage mechanics. *International Journal of Fatigue* 73: 66–76.
- Hojjati-Talemi R, Abdel Wahab M, De Pauw J, et al. (2014) Prediction of fretting fatigue crack initiation and propagation lifetime for cylindrical contact configuration. *Tribology International* 76: 73–91.
- Kachanov LM (1986) *Introduction to Continuum Damage Mechanics*. Boston, Dordrecht: Martinus Nijhoff Publisher.
- Kang G, Liu Y, Ding J, et al. (2009) Uniaxial ratcheting and fatigue failure of tempered 42CrMo steel: Damage evolution and damage-coupled visco-plastic constitutive model. *International Journal of Plasticity* 25: 838–860.
- Lemaitre J (1985) A continuous damage mechanics model for ductile fracture. *Journal of Engineering Materials and Technology* 107(1): 83–89.
- Lemaitre J and Chaboche JL (1990) *Mechanics of Solid Materials*. Cambridge: Cambridge University Press.
- Lemaitre J and Rodrigue D (2005) *Engineering Damage Mechanics: Ductile, Creep, Fatigue and Brittle Failures*. Berlin Heidelberg: Springer-Verlag, pp. 35–36.
- Madge JJ, Leen SB, McColl IR, et al. (2007) Contact-evolution based prediction of fretting fatigue life: Effect of slip amplitude. *Wear* 262: 1159–1170.
- Murakami S (2012) *Continuum Damage Mechanics: A Continuum Mechanics Approach to the Analysis of Damage and Fracture*. New York: Springer.
- Oskouei RH and Chakherlou TN (2009) Reduction in clamping force due to applied longitudinal load to aerospace structural bolted plates. *Aerospace and Science and Technology* 13: 325–330.
- Oskouei RH and Ibrahim RN (2012) Improving fretting fatigue behaviour of Al 7075-T6 bolted plates using electroless Ni-P coatings. *International Journal of Fatigue* 44: 157–167.
- Ruiz C, Boddington PHB and Chen KC (1984) An investigation of fatigue and fretting in a dovetail joint. *Experimental Mechanics* 24: 208–217.
- Shen F, Hu W and Meng Q (2015b) A damage mechanics approach to fretting fatigue life prediction with consideration of elastic-plastic damage model and wear. *Tribology International* 82: 176–190.
- Shen F, Hu W, Voyiadjis GZ, et al. (2015a) Effects of fatigue damage and wear on fretting fatigue under partial slip condition. *Wear* 338: 394–405.
- Szolwinski MP and Farris TN (1998) Observation, analysis and prediction of fretting fatigue in 2024-T351 aluminum alloy. *Wear* 221: 24–36.

- US Department of Defense (1998) *Military Handbook-MIL-HDBK-5H: Metallic Materials and Elements for Aerospace Vehicle Structures*. Knovel interactive ed. Washington DC, US: US Department of Defense, pp. 3–379.
- Vingsbo O and Söderberg S (1988) On fretting maps. *Wear* 126: 131–147.
- Voyiadjis GZ and Echle R (1998) High cycle fatigue damage evolution in uni-directional metal matrix composites using a micro-mechanical approach. *Mechanics of Materials* 30: 91–110.
- Voyiadjis GZ and Kattan PI (2005) *Damage Mechanics*. Boca Raton: Taylor & Francis.
- Voyiadjis GZ and Kattan PI (2006) Damage mechanics with fabric tensors. *Mechanics of Advanced Materials and Structures* 13(4): 285–301.
- Voyiadjis GZ and Kattan PI (2008) A comparative study of damage variables in continuum damage mechanics. *International Journal of Damage Mechanics* 18(4): 315–340.
- Voyiadjis GZ and Thiagarajan G (1995) An anisotropic yield surface model for directionally reinforced metal-matrix composites. *International Journal of Plasticity* 11(8): 867–894.
- Zhang T, McHugh PE and Leen SB (2012) Finite element implementation of multiaxial continuum damage mechanics for plain and fretting fatigue. *International Journal of Fatigue* 44: 260–272.
- Zhu Y, Kang G, Ding J, et al. (2013) Study on bending fretting fatigue of LZ50 axle steel considering ratcheting by finite element method. *Fatigue and Fracture of Engineering Materials and Structures* 36: 127–138.